HHS Public Access

Author manuscript

Matrix Biol. Author manuscript; available in PMC 2017 May 01.

Published in final edited form as:

Matrix Biol. 2016 ; 52-54: 29–42. doi:10.1016/j.matbio.2016.03.005.

Makings of a brittle bone: Unexpected lessons from a low protein diet study of a mouse OI model

E.L. Mertz[*,a], **E. Makareeva**[*,a], **L.S. Mirigian**[*,a], **K.Y. Koon**[a], **J.E. Perosky**[b], **K.M. Kozloff**[b], and **S. Leikin**[a]

[a]Section on Physical Biochemistry, Eunice Kennedy Shriver National Institute of Child Health and Human Development, National Institutes of Health, Bethesda, MD 20892, USA

[b]Department of Orthopaedic Surgery, University of Michigan, Ann Arbor, MI 48109, USA

Abstract

Glycine substitutions in type I collagen appear to cause osteogenesis imperfecta (OI) by disrupting folding of the triple helix, the structure of which requires Gly in every third position. It is less clear, however, whether the resulting bone malformations and fragility are caused by effects of intracellular accumulation of misfolded collagen on differentiation and function of osteoblasts, effects of secreted misfolded collagen on the function of bone matrix, or both. Here we describe a study originally conceived for testing how reducing intracellular accumulation of misfolded collagen would affect mice with a Gly610 to Cys substitution in the triple helical region of the α2(I) chain. To stimulate degradation of misfolded collagen by autophagy, we utilized a low protein diet. The diet had beneficial effects on osteoblast differentiation and bone matrix mineralization, but it also affected bone modeling and suppressed overall animal growth. Our more important observations, however, were not related to the diet. They revealed how altered osteoblast function and deficient bone formation by each cell caused by the G610C mutation combined with increased osteoblastogenesis might make the bone more brittle, all of which are common OI features. In G610C mice, increased bone formation surface compensated for reduced mineral apposition rate, resulting in normal cortical area and thickness at the cost of altering cortical modeling process, retaining woven bone, and reducing the ability of bone to absorb energy through plastic deformation. Reduced collagen and increased mineral density in extracellular matrix of lamellar bone compounded the problem, further reducing bone toughness. The latter observations might have particularly important implications for understanding OI pathophysiology and designing more effective therapeutic interventions.

Keywords

osteogenesis imperfecta; bone; mineralization; collagen; Raman microspectroscopy; biomechanics

Corresponding author: Sergey Leikin, NICHD, NIH, Bldg. 9, Rm. 1E-127, Bethesda, MD 20892, USA, leikins@mail.nih.gov.

*These authors contributed equally to the design of the study and interpretation of the results.

Introduction

Osteogenesis imperfecta (OI)[1], also known as the “brittle bone disease”, is a heterogeneous group of heritable bone disorders characterized by abnormal formation, deformities and fragility of bones [1]. Similar to other rare skeletal diseases, OI studies identify molecules and pathways essential for bone development in general and might provide valuable insights for treatment of more common pathologies [2]. Many novel OI mutations in different genes have been discovered in recent years [1, 3, 4]. Yet, most OI patients have autosomal dominant mutations in the genes coding for α1(I) and α2(I) chains of of type I collagen, which is the main building block of organic bone matrix. Furthermore, most cases of severe OI result from substitutions for an obligatory Gly in the sequence of repeating Gly-X-Y triplets of type I collagen triple helix (X and Y are variable amino acids in this sequence).

Hundreds of substitutions for Gly have been described (http://www.le.ac.uk/ge/collagen/), but it is still unclear what makes some of them more severe than others and why the same substitution might result in mild, severe or lethal outcome in different patients [1, 5]. It is unclear whether Gly substitutions cause OI by altering differentiation and function of bone-producing cells (osteoblasts) that synthesize procollagen, by affecting collagen function in bone matrix outside the cells, or by doing both [1]. It is also unclear how the underlying molecular processes affect the amount, geometry and density of bone as well as why OI bones are brittle.

To test the role of osteoblast malfunction in OI, we conducted a pilot study of a low protein (LP) diet effect on heterozygous Col1a2$^{tm1Mcbr/J}$ (G610C) mice. This mouse model has a Gly610 to Cys substitution in the triple helical region of the α2(I) chain of type I collagen, resulting in moderate OI [6]. It is commercially available (Jackson Laboratories, Stock No: 007248) and has been utilized in several OI studies [6-10]. G610C mice mimic the mutation and OI phenotype found in a large group of related patients from an Old Order Amish community in Lancaster County, PA. As expected for most Gly substitutions [11], the G610C mutation disrupts folding of the procollagen precursor of type I collagen and causes accumulation of misfolded procollagen in the Endoplasmic Reticulum (ER), resulting in cell stress and osteoblast malfunction [7]. LP diet was selected as a simple approach to activating autophagy [12] with an expected additional effect of reducing overall procollagen synthesis (and therefore misfolding) by osteoblasts. Since earlier studies suggested that autophagy might play a key role in degradation of misfolded procollagen in OI [7, 13, 14], our objective was to see how an LP diet would affect the bone material before initiating more complex studies of more precise autophagy targeting. We combined multiple approaches to analyzing bone material properties in order to distinguish different LP diet effects on bone synthesis, structure and mineralization. We found closer to normal mineralization of bone matrix in G610C mice, although other diet effects reduced the net bone strength. Most surprisingly, we observed a long-lasting beneficial effect of the diet on bone marrow stromal

[1]Abbreviations: BMD – bone mineral density, BMSC – bone marrow stromal cell, CFU – colony forming units, CFUALP– alkaline phosphatase positive CFU, CFU-F – fibroblast-like CFU, CFU-OB – mineralizing (osteoblast-like) CFU,CNF – CaCl-NaCl-NaF solution (2 mM CaCl2, 150 mM NaCl, 10 μm NaF pH~7.5), ER – endoplasmic reticulum, HDIR –high definition infrared, Het – heterozygous G610C, LP – low protein, MAR – mineral apposition rate, MOR –mineral:organics ratio, OI – osteogenesis imperfecta, RP – regular protein, SD – standard deviation, SE – standard error of the mean value, TMD – tissue mineral density, Wt – wild type

cells from G610C animals after they were cultured *in vitro* at normal conditions without nutrient deprivation. Based on the observed LP diet effects, we are now conducting a more refined and precise study of autophagy manipulation with genetic tools.

In the present paper, however, we focus primarily on our other, unanticipated findings that might have more general and important implications for understanding mechanisms of bone fragility in OI irrespective of the dietary treatment. Specifically, we discuss how the mutation disrupts bone modeling process, affects matrix composition and mineralization, and reduces bone toughness.

Results

LP diet treatment

At 8 weeks of age, 5 wild type (Wt) and 5 heterozygous G610C (Het) male animals were put on 18% protein (regular protein, RP) diet. At the same time, 5 Wt and 5 Het male animals were placed on 8% protein (low protein, LP) diet. The latter diet was supplemented with Met, Phe, Tyr, Trp, and carbohydrates and had the same, 3.8 Kcal/g energy content. At the start of the diets, the animals were injected with calcein, a fluorescent dye which binds to mineralized bone surfaces. The animals were given a second calcein injection at 11 weeks of age and a third calcein injection at 16 weeks of age. They were sacrificed at 17 weeks of age while remaining on the 18% and 8% diets.

Bone quantity, geometry and strength

4 point bending tests of femurs from RP diet animals (Fig. 1) revealed statistically significant reduction in energy to failure, plastic component of this energy, and plastic (post-yield) displacement in Het mice. The other parameters were not significantly affected. Het bone had normal stiffness as well as normal yield load and ultimate load. The dramatically decreased bone plasticity indicated increased bone brittleness and reduced ability to absorb deformation energy.

μCT analysis of femurs (Fig. 2) revealed reduced number and density of trabeculae in Het mice, but their thickness and tissue mineral density (TMD) were within one standard deviation (SD) from Wt averages. The only statistically significant abnormality of the cortical bone in Het mice was slightly higher overall bone mineral density (BMD) and TMD. Cortical perimeters, thickness, bending moments of inertia (anterior-posterior, Ixx and medial-lateral, Iyy), and torsional moment of inertia (Izz) were all within 1 SD of Wt averages. These changes in bone architecture and mineralization were consistent with minimal effect of the mutation on the elastic response and ultimate load in the 4 point bending test at mid-diaphysis (the region of femur with almost no trabecular bone). The observed minor hypermineralization of cortical bone could contribute to the brittleness of Het femurs, but appeared unlikely to be responsible for the whole effect, given the dramatic change in the bone plasticity.

LP diet significantly suppressed overall animal growth in both genotypes, as indicated by reduced weight gain, and inhibited cortical drift, complicating the analysis of bone geometry

and mechanical strength and precluding straightforward comparison of these parameters with RP diet animals (Supplementary Fig. S1).

Cortical bone structure

Polarized microscopy of cortical bone sections from mid-diaphysis revealed significant differences in bone matrix organization within Wt and Het cortical bone (Fig. 3). In 4 m.o. Wt animals, we consistently observed lamellar bone at anterior endosteal and posterior periosteal side and woven as well as parallel-fibered (aka fine-fibered and parallel-fibered, finely bundled [15, 16]) bone at anterior periosteal and posterior endosteal side. Age-matched Het animals had lamellar bone at both anterior and posterior cortical surfaces and woven bone in the middle. The amount of poorly ordered and likely more fragile woven bone [17-19] was larger in every section from Het vs. Wt animals. Increased content of woven and reduced content of lamellar bone in Het animals was also observed at 10 month age (Supplementary Fig. S2).

Calcein labeling showed that the increased content of woven bone in Het mice resulted from disruption of normal cortical drift (Fig. 3). Posterior deposition and anterior resorption of cortical bone [20] replaces immature woven with more mature lamellar bone in adult mice. This anterior-to-posterior cortical drift pattern appeared to be disrupted in Het mice, in which we observed inconsistent, variable deposition of new bone at all posterior and anterior surfaces, resulting in entrapment and accumulation of immature woven and parallel-fibered bone. The mineral apposition rate (MAR) measured from the distance between the calcein lines appeared to be smaller in Het mice at similar sites (Supplementary Fig. S3), although average MAR values were not quantified. In the context of our experiment, quantitative analysis of average MAR was difficult and potentially misleading because of large MAR variation from site to site and disruption of the bone modeling pattern in Het animals. The normal cortical bone thickness in Het mice appeared to be maintained due to deposition of new bone at more sites on both sides of the cortical layer.

Cortical bone mineralization

Because of the differences in the content of different types of bone and the pattern of their deposition, the average TMD of the cortical layer might not accurately represent the potential effect of the increased mineral density on bone fragility. Heterogeneous mineralization of woven bone might skew the average values, masking important differences in mineralization of mature lamellar bone. We therefore examined mineralization profiles in calcein-labeled lamellar bone in a posterior periosteal layer, in which we could compare the same type of bone deposited at the same age in both Wt and Het animals (Fig. 4A,B).

Raman micro spectroscopy revealed that the complete mineralization took ~6 weeks after deposition of the organic bone matrix and that femurs from our 17 week old animals contained substantial amounts of incompletely mineralized lamellar matrix. The mineral:organics (organic matrix molecules) ratio (MOR) increased to 50-70% of the final value within 1 week of matrix deposition followed by slow further mineralization (Fig. 4B). To discriminate the equilibrium properties of bone matrix and avoid potentially complex

effects of variations in mineralization kinetics, we focused subsequent measurements on completely mineralized bone regions.

We found that the mineral content of completely mineralized, mature lamellar bone matrix was ~ 15% higher in Het compared to Wt RP diet animals (Fig. 4D), i.e. 3-4 times larger than the average TMD difference. LP diet partially normalized mature lamellar bone mineralization in Het animals by reducing the excessive mineral deposition, as indicated by MOR comparison in adjacent regions of bone deposited before and after the start of the diet (Fig. 4E). This improvement of bone material properties did not appear to be associated with slower matrix synthesis by nutrition-deprived osteoblasts, since we found no clear correlation between MAR and mineral content at different sites within lamellar bone in the same animal (Supplementary Fig. S3).

From the difference between Het:Wt ratios for MOR and TMD, we deduced that the density of organic matrix molecules was 5-15% lower in Het vs. Wt bone (Table 1, Supplementary Data Analysis). This reduction was primarily due to reduced collagen density, since collagen accounts for close to 90% of all organic material in bone and the collagen:organics ratio was unchanged or even reduced in Het mice (Table 1). Not only lower density of collagen in OI bone could reduce bone plasticity, but it would provide more space for extrafibrillar mineral deposition and therefore increased MOR and TMD (Fig. 5C), as hypothesized previously [21]. The reproducibility of collagen Raman peak intensities was not sufficient for direct collagen density measurements. Yet, high-definition infrared (HDIR) imaging of collagen in matrix deposited by calvarial osteoblasts in culture supported this interpretation (Fig. 5A,B).

Osteoblast differentiation and function

Altered structure, composition and deposition pattern of bone matrix as well as the LP diet effect on matrix mineralization indicated abnormal differentiation and/or function of Het osteoblasts, consistent with our study of G610C neonates and calvarial osteoblasts [7]. Electron microscopy (EM) of lumbar (L2) vertebrae confirmed severe dilation of ER cisternae in Het osteoblasts, apparently caused by accumulation of misfolded mutant collagen molecules inside the ER (Fig. 6A). However, we could not deduce a clear LP diet effect on ER dilation because of highly variable ER appearance in different cells (Supplementary Fig. S4).

Quantitative real-time PCR (qPCR) analysis of mRNA extracted from calvaria showed no statistically significant differences between the RP and LP diet groups, but it revealed abnormal transcription pattern of osteoblast genes in Het animals (Fig. 6B, Supplementary Fig. S5). Higher transcription of *Col1a1*, *Col1a2*, *Serpinh1* (HSP47), and *Bglap* (osteocalcin) relative to osteoblast precursor genes (*Runx2* and *Sp7*) as well as to endogenous control (*Hprt1*) was consistent with increased bone formation surface (Fig. 3C), suggesting increased osteoblastogenesis. At the same time, the lack of accompanying increase in the transcription of *Ibsp* (bone sialoprotein) and *Dmp1* indicated deficient osteoblast maturation.

Deficient osteoblast maturation was further supported by analysis of osteoblast differentiation from bone marrow stromal cells (BMSC) in culture (Fig. 6C). We observed a

dramatic reduction (6 fold, > 2 SD) in the number of mineralization-capable osteoblast colonies (CFU-OB) from Het RP diet animals ($p<0.05$) but not from Het LP animals (see Supplementary Table S5 for statistical analysis). The number of alkaline phosphatase-positive colonies (CFU-ALP) and total number of colonies (CFU-F) of Het BMSCs was within 1 SD of Wt BMSCs, regardless of the diet. Remarkably, LP diet treatment appeared to increase and almost completely normalize CFU-OB without affecting CFU-ALP or CFU-F in BMSCs cultured at the same conditions as the cells from RP diet mice (Fig. 6C, lower panel). Note, however, that the p-value for the CFU-OB increase in Het LP BMSCs compared to Het RP BMSCs was borderline-significant ($p=0.07$, Supplementary Table S5).

Discussion

Study design and limitations

Consistent with our initial hypothesis, the LP diet had beneficial effects on osteoblast differentiation (Fig. 6C) and mineralization of the newly deposited bone (Fig. 4E) in G610C mice. At the same time, it suppressed overall animal growth, reduced mineral apposition rate, and reduced the absolute bone strength and toughness in both genotypes, demonstrating detrimental net effect of prolonged LP diet on bones during animal growth (Supplementary Fig. S1 and S3).

Although this study was conceived as a pilot LP diet test, subsequent data analysis revealed important features of osteoblastogenesis, bone modeling, and bone strength and toughness in G610C mice irrespective of the diet. We believe that our unanticipated findings might have important implications for (a) understanding causes of bone fragility in OI, (b) analysis of animal OI models and translation of the result to clinical applications, and (c) understanding and targeting osteoblast cell stress in OI and other bone disorders.

Before interpreting these findings, we should outline the limitations stemming from the mismatch in the original design and outcome of the study. We could not justify including additional animals into the study given the detrimental net effect of the LP diet, which prevented us from following up on some of our observations (e.g. performing accurate quantitative measurements of average MAR or utilizing the same rather than different bone types for systematic analysis by different methods). The limited sample size of 5 animals per group also restricted the statistical power of our conclusions. We could interpret only the observations that were qualitatively clear or quantitatively significant (see Supplementary Tables 1-5 for full statistical analysis). Thus, below we discuss only the effects that either meet these criteria or are sufficiently small for concluding that they are within the normal range of variation (< 1 SD). For instance, we could not justify looking for possible differences between Wt and Het cortical geometry, since over 64 mice/group would be required for detecting 0.5 SD effects.

Bone fragility in adult G610C mice

Susceptibility to fractures in OI, which is also known as the “brittle bone disease”, is caused by insufficient deposition, abnormal organization, and increased fragility of bone material

[1]. Separating the contributions from these distinct deficiencies, which usually occur together, is important for understanding the disease and developing treatments.

The amount and geometry (perimeter, thickness and moments of inertia, Fig. 2) as well as elasticity (yield load and stiffness, Fig. 1) of the cortical bone in our Het mice were all within the normal range of variation for Wt mice. Curiously, significantly different observations for mice of the same age and genetic background were reported in [10]. In particular, our measurements of cortical thickness (C.Th) and torsional moment of inertia (Izz) in Wt mice on RP diet yielded C.Th=0.22±0.02 mm and Izz=0.55±0.16 mm^4 (N=5) compared to C.Th=0.39±0.02 and Izz=0.87±0.12 (N=9) in [10]. C.Th and Izz in our Wt and Het mice were within 1 SD of each other while ~2 SD difference between Wt and Het mice was observed in [10]. We cannot attribute these differences to the sample size or experimental error in either of the two studies. Statistical power and probability calculations suggest that 3 animals would already be sufficient for validating ~10 SD, $p<0.001$ difference in Wt C.Th and 5 animals are sufficient for validating ~2.3 SD, $p=0.0011$ difference in Wt Izz. We can only speculate that these differences might be related to animal housing, diet, genetic drift or seasonal variations.

Remarkably, because of the similar cortical geometry, the reduced femur toughness in our Het mice, which require ~ 2 times lower energy for mid-shaft fracture (failure energy in Fig. 1) can be attributed entirely to 3-5 times lower than normal plastic displacement prior to failure and 3-5 times lower energy absorbed by this displacement (Fig 1). In other words, the fragility of Het femurs is caused by the brittleness of the cortical bone material. (Note that the reduced number of trabeculae and density of Het trabecular bone (Fig. 2) might affect the strength of femur metaphyses, but the 4-point bending performed here tests femur diaphysis, which has very little trabecular bone.)

One important factor in the cortical bone brittleness in Het mice is altered bone modeling (Figs. 3,4). Instead of normal anterior-to-posterior cortical drift that replaces woven with lamellar bone in mouse femurs, Het G610C osteoblasts deposit bone on all anterior and posterior surfaces, trapping the immature woven and parallel-fibered bone between endosteal and periosteal layers (Fig. 3). The immature bone has poor organization of collagen fibers and is expected to be more brittle [17-19]. The altered bone modeling process compensates for the reduced matrix synthesis and mineral apposition rate by Het osteoblasts, normalizing the amount, geometry and stiffness of the bone. However, this adaptation comes at the cost of immature (woven) bone entrapment that contributes to the reduced ability of the bone to absorb energy without fracturing. Interestingly, heterozygous Brtl mice with a G349C substitution in the α1(I) chain [22] have reduced mineral apposition rate but normal cortical drift pattern, resulting in altered bone geometry and reduced bone mass [20].

Another factor is increased mineral content and reduced collagen density (Figs. 2,4,5, Table I). Increased bone mineralization (volumetric mineral density within bone matrix, aka TMD) is a common feature of OI [23], which is also observed in Brtl animals [24]. Yet, overall TMD is difficult to interpret mechanistically, because bone regions with different matrix structure and maturity have different mineral content; e.g. TMD might be affected by the

content of woven bone and rate of bone deposition. We therefore examined mineralization of mature lamellar bone and found that its mineral content was increased in Het G610C mice (Fig. 4D).

Contrary to our expectation, the mineral content of mature lamellar bone did not correlate with MAR and thus with the overall rate of collagen production at different sites along bone surface in either Wt or Het animals (Fig. 4F). One possible explanation of this observation would be that the quality of matrix produced by an individual cell does not correlate with the collagen synthesis rate by this cell. It is also possible that this correlation is obscured by variations in osteoblast density and differentiation stages at different bone surface sites.

In addition, our observations revealed reduced density of organic matrix molecules (Table I), supporting the hypothesis of increased mineralization proposed in [21]. Within this hypothesis, the decreased density of organic matrix provides additional space that is completely filled by mineral (Fig. 5C). Since collagen fraction in the organic matrix is unchanged or even reduced (Table I), the reduced organics density also indicates reduced density of collagen fibers and suggests that the hypermineralization of Het bone might be caused by increased extrafibrillar mineral deposition.

In principle, the reduced density of collagen fibers might increase bone brittleness even more than the resulting hypermineralization. Collagen fibers enable bone to absorb impact energy through their elastic deformation and rupture in micro-cracks that develop during plastic bone deformation prior to failure. The importance of collagen for bone strength, particularly during plastic deformation was identified already in early publications [25, 26]. Different types of collagen content measurements in bone and osteoblast cultures have been performed in the context of OI studies (see e.g., [27, 28]), but typically a ratio of collagen to other bone components rather than the volumetric density of collagen fibers in the bone matrix is reported. Here we estimate that lamellar cortical bone in Het G610C mice has ~ 10% lower collagen fiber density compared to Wt mice (Table I, Fig. 5). Because the relationship between collagen fiber density and bone strength is poorly understood, it is presently unclear how big is the contribution of this relatively small change in collagen density to the observed loss of bone plasticity (Fig. 1).

Implications for human OI

Understanding effects of OI mutations on the properties of mature lamellar bone is particularly important for translating mouse model findings to human OI. Mouse bone homeostasis has several distinct features that are different from humans. Adult mouse bone contains substantial woven and parallel-fibered regions within the cortical layer. These regions are poorly structured and likely to affect bone mechanics [17-19]. In contrast, human cortical bone is predominantly (if not entirely) lamellar from an early age, even in the case of classical OI caused by collagen mutations [29]. In humans, osteons constantly remodel and replace poorly structured and fatigued material with new lamellar bone inside the cortical layer [15]. In mice, intra-cortical bone remodeling is very limited, so that the existing bone material is replaced and renewed primarily in the process of cortical drift. As illustrated here, measurements of average structure, mineralization and mechanics of whole mouse bone might not accurately represent the corresponding properties of lamellar regions.

The present study provides an approach to elucidating the structure and composition of the latter.

Like in G610C mice, altered modeling and composition of bone matrix are expected to affect human bone, but their relative contribution and the context in which they are important might be different. In particular, hypermineralization and reduced collagen fiber density might affect the material properties of human bone more than disruptions in bone modeling. Because of osteons, entrapment of woven bone is less likely in human OI than in mice. Abnormal bone modeling might be more important for altering bone geometry and preventing restoration of normal bone shape after fractures that heal with angulations, which are typical features of human OI [30]. In addition, we can only speculate whether a variety of different human OI mutations would have similar effects on bone to the α2(I)-G610C substitution modeled by G610C mice.

Targeting osteoblast cell stress

At the scale of individual molecules and cells, essentially the same basic processes of bone matrix synthesis are involved in different types of bone modeling and remodeling in mice and humans. Collagen mutations affect these processes in two ways: (a) They cause malfunction of secreted mutant molecules outside the cells. (b) They cause malfunction of osteoblasts, which have difficulty producing and secreting mutant molecules. From a practical perspective, prevention of extracellular collagen malfunction requires altering expression of mutant collagen by gene or cell therapy, which is extremely difficult. In contrast, osteoblast malfunction might be at least partially corrected through much simpler therapeutic approaches.

In the G610C mouse model, separate analysis of neonates [7] and the present study of adult animals suggest that osteoblast malfunction plays a major role in bone pathology. Delayed folding and intracellular retention of procollagen [7] combined with severe ER dilation ([7], Fig. 6A) suggest accumulation of misfolded procollagen in osteoblast ER. The resulting cell stress is revealed by increased EIF2α phosphorylation and *Ddit3* (CHOP) transcription [7]. It alters osteoblast differentiation, ability to deposit matrix, and response to crucial signaling pathways [7]. Adult G610C animals appear to adapt by upregulating osteoblast formation, as suggested by increased bone formation surface (Fig. 3) and increased transcription of genes expressed in osteoblasts (*Runx2, Sp7, Ibsp, Bglap B, Ifitm5*, and *Dmp1*) relative to *Hprt1* expressed in all cells (Fig. 6B). However, increasing collagen synthesis and accompanying accumulation of misfolded molecules appear to prevent proper osteoblast maturation, as suggested by reduced transcription of *Ibsp* (bone sialoprotein), *Ifitm5* (Bril), and *Dmp1* relative to *Col1a1*, *Col1a2* and *Bglap B* (osteocalcin) *in vivo* as well as by reduced CFU-OB *in vitro* (Fig. 6B,C). Increased osteoblastogenesis allows the animals to deposit normal amount of cortical bone, but at the cost of altered bone modeling process. Compounding the problem, osteoblast malfunction leads to deposition of lower quality, hypermineralized bone matrix (Fig. 4D).

Accumulation of misfolded procollagen in the ER [31] and abnormal differentiation of osteoblasts [13] were also observed in the Brtl mouse model of OI. In both the G610C and Brtl mouse OI models, the misfolded procollagen is degraded by autophagy [7, 13] and its

accumulation causes some form of cell stress response, as indicated by upregulation of a key cell stress response gene *Ddit3* [7, 32]. Yet, the resulting effect on bone formation has both similar (e.g. deficient deposition and hypermineralization) and distinct (e.g. abnormal cortical drift) features, which might be caused by differences in the effects of the mutant molecules on the osteoblast function, on the properties of the extracellular matrix, or on both.

A reduction in mature lamellar bone hypermineralization after LP diet treatment (~35% of the difference between MOR in Wt and Het bone, Fig. 4D,E) seems to support the idea that bone material properties might be improved by targeting osteoblast cell stress in OI. This effect was not a trivial consequence of the reduction in the rate of bone matrix synthesis by nutrient deprivation, since the mineral content did not depend on the matrix synthesis rate at different sites (Fig. 4F). Most likely it was associated with increased intracellular degradation of misfolded procollagen caused by autophagy that was shown [12] to be stimulated by LP diet. The rather crude nutrient deprivation caused by prolonged LP diet was unlikely to completely alleviate the osteoblast cell stress, e.g. because nutrient deprivation might cause its own stress in secretory cells. Hence, it should not be surprising that we did not observe any major effects of LP diet on osteoblast ER dilation or abnormal expression of osteoblast-specific genes in Het animals, consistent with only partial improvement in matrix quality.

Crucially, a rescue of osteoblast differentiation in normal nutrient culture of BMSCs from LP diet Het animals (Fig. 6C), indicates that autophagy stimulation has a lasting effect after the nutrient stress is removed. Autophagy activation in Het BMSCs appears to last long enough to even affect the cell differentiation in subsequent culture, probably because it becomes epigenetically programmed. Consistently, differentiation of BMSCs from Wt animals was not affected by the LP diet treatment. This interpretation of the BMSC differentiation rescue is further supported by the fact that the LP diet treatment affected only the colonies of cells actively producing collagen (CFU-OB) but not the colonies of other cells (Fig, 6C). While still speculative, it provides sufficient impetus for careful testing of more specific and permanent autophagy activation in osteoblasts by genetic means without the side effects of dietary or drug treatment, which is currently under way in our laboratory. It also provides hope that a regimen of diet and drugs with beneficial, lasting effects of autophagy activation and minimal or no side effects of nutrient/drug-induced cell stress can be found.

In conclusion, it is worthwhile to recall that procollagen misfolding in the ER might be caused not only by mutations in collagen and collagen chaperones but also by disruptions in the overall ER health, which is affected by aging, inflammation and other factors (see, e.g. [33] and references therein). Misfolded procollagen accumulation might therefore contribute to osteoblast malfunction associated with age, cancer treatment or other conditions. A particularly appealing approach is to enhance the ability of the cell to degrade misfolded procollagen via autophagy, reducing the misfolded procollagen load. This approach might improve the quality of bone material unlike the existing treatments that focus on increasing the bone quantity. While designed to be simple and crude, our LP diet study provides sufficient evidence for pursuing this strategy.

Experimental Procedures

Animals

Het G610C mice (B6.129(FVB)- Col1a2$^{tm1Mcbr/J}$) were purchased from Jackson Laboratories (stock # 007248) and maintained on the C57BL/6J background. Isocaloric (3.8 kcal/g, 9.3:1 carbohydrate:fat ratio) LP (92 g casein per 1,000 g supplemented with 1.2 g Met, 5.0 g Phe, and 5.3 g Tyr, 1.1 g Trp) and RP (207 g casein per 1,000 g) diets (cat. # TD. 110721 and TD.110722, respectively) were formulated, prepared and sterilized by irradiation at Harlan Laboratories. All Wt and Het animals in the LP and RP diet groups were genotyped, housed and treated at Jackson Laboratories. At 8, 11, and 16 weeks of age, the animals were weighted followed by intraperitoneal injection of 20 μg/g body weight calcein (Sigma)in 1.4% $NaHCO_3$. The dietary treatment was started immediately after the first calcein injection. The animals were shipped for tissue and BMSC collection several days after the last calcein injection. They were euthanized at an NIH animal facility one week after the last injection, within 2 days after arrival. Tissues and cell cultures from these animals were used for all of the experiments described in this paper. The only exception was qualitative imaging of cortical bone structure in femurs from 10 m.o. mice (Supplementary Fig. S2), for which we used mice housed at an NIH animal facility and fed a regular diet. For these experiments, subcutaneous injections of 10 μg/g body weight calcein in 1.4% $NaHCO_3$ were performed as described in Supplementary Fig. S2. All animal care and experiments were performed in accordance with protocols approved by the NICHD and Jackson Laboratories ACUC.

Biomechanics and μCT

Right femurs were excised from euthanized LP and RP diet animals. After removal of surrounding muscles, the femurs were wrapped in PBS-soaked gauze, and stored at -20 °C. The femurs were analyzed by μCT and 4-point bending tests as described in [20, 24]. Briefly, femora μCT (eXplore Locus SP, GE Healthcare) images were acquired in water at 0.5° angle of increment and 4 frames averaged, using 80 kV/80μA source projected through a 0.508 mm Al filter to reduce beam hardening and a custom beam flattener. The images were reconstructed at 18 μm isotropic voxel size. Cortical regions of interest (ROI) were 15% of total femoral length, centered midway between the distal femoral growth plate and the lateral third trochanter. Distal femoral trabecular ROIs were adjacent to the distal femoral growth plate, extending proximally 10% of the total femoral length. Fixed thresholds of 2000 HU for cortical bone and 1350 HU for trabecular bone were used to segment bone from non-bone for analysis. Cortical thickness, periosteal and endosteal perimeters, bending moments of inertia across the anterior-posterior axis (Ixx), medial-lateral axis (Iyy), torsional moments of inertia (Izz), BMD (total bone mineral content normalized by volume of interest), and TMD (bone mineral content normalized by bone volume) were quantified with vendor-supplied software (MicroView v2.2, GE Healthcare).

Following μCT, femora were tested in four-point bending to failure (MTS 858, MiniBionix) with the posterior surface under tension at a load rate of 0.5 mm/sec, upper support distance 6.26 mm, and lower support distance 2.085 mm. Bending force applied in the direction corresponding to Iyy was monitored with a 50 lb load cell (Sensotec) and resulting

displacement was monitored by an external linear variable differential transducer (LVDT, Lucas Schavitts). A custom MATLAB code was used to calculate all mechanical parameters measured from load-displacement data.

BMSC isolation and culture

Bone Marrow Stromal Cells (BMSCs) were isolated from left femurs of LP and RP diet animals as described in [7, 34] and plated at 20,000 nucleated cells/10cm^2 for CFU-F and CFU-ALP and at 100,000 nucleated cells/10 cm^2 for CFU-OB in sextuplicate. The cells were cultured in αMEM (Life Sciences) supplemented with GlutaMAX™ (Life Sciences), 20% Fetal Bovine Serum from a preselected lot (Valley Biomedical, Catalog # BS3033, Lot # 2C0550), 100 μM ascorbic acid 2-phosphate (Sigma), 1 nM dexamethasone (Sigma), and 1% Pen-Strep (Life Sciences) at 37 °C, 5% CO_2 and 5% O_2. On day 14, the cells were stained with Alkaline Phosphatase Kit (Sigma) for CFU-ALP (colonies with 15+ positive cells) and then re-stained with Crystal Violet (Sigma) for CFU-F (20+ cell colonies). For CFU-OB (50+ cell colonies with mineralized matrix), the cells were cultured from day 14 to day 28 in the same medium supplemented with 10 nM dexamethasone and 5mM β-glycerol phosphate (Sigma) with regular media changes, fixed with 10% formalin (Sigma) and stained with Alizarin Red S (Sigma).

Gene expression analysis

RNA was extracted from frontal bones of LP and RP diet animals with Trizol (Life Sciences), purified with Direct-zol RNA MiniPrep (Zymo Research) and reverse transcribed with SuperScript III Supermix (Life Sciences), using random hexamers as primers. Relative mRNA concentrations were measured in a 7500 Fast Real Time PCR system (Applied Biosystems) with Taqman gene expression assays (*Bglap B*, Mm03413826_mH; *Col1a1*, Mm00801666_g1; *Col1a2*, Mm00483888_m1; *Dmp1*, Mm01208363_m1; *Hprt1*, Mm01545399_m1; *Ibsp*, Mm00492555_m1; *Ifitm5*, Mm00804741_g1; *Runx2*, Mm00501584_m1; *Serpinh1*, Mm00438058_g1; and *Sp7*, Mm00504574_m1). The results were analyzed based on ΔC_T values at the same threshold for all samples.

Sectioning of bone and cultured cell/matrix layer

After BMSC extraction, left femurs were fixed overnight at room temperature in freshly prepared 0.7% formaldehyde, 0.7 × phosphate buffered saline (PBS, Life Sciences), and 0.5 mM $CaCl_2$, using Pierce™ 16% methanol-free formaldehyde sealed under nitrogen (Thermo Scientific). Anterior and posterior sides of femur mid-diaphysis (Fig. 3B) were sawed with a spinning diamond disk and cryo-sectioned without dehydration or demineralization, following a procedure optimized for mineralized bone [35]. Specifically, the sawed pieces were embedded in 20 wt%-10 kDa / 15 wt%-360 kDa polyvynilpyrrolidone (Sigma) cryosectioning media, and sectioned at −25°C with a D-profile tungsten carbide knife. The section plane was parallel to the femur axis and perpendicular to exterior femur surface (Fig. 1). The resulting 10 μm sections were either mounted in Permount medium (Thermo Scientific) on glass slides for microscopic observations or washed briefly in PBS, and sealed with PBS between quartz slide and coverslip for microscopic and Raman micro-spectroscopic measurements.

Parietal bone osteoblasts were isolated from 3-8 day old Het G610C and Wt pups and cultured in a growth medium (αMEM supplemented with GlutaMAX™, 10% VB-FBS, 100 μM ascorbic acid 2-phosphate, and 1% Pen-Strep) at 37 °C, 5% CO_2 and 5% O_2 for 3 weeks with media changes every 2-3 days. The resulting matrix layer was fixed in 0.7% formaldehyde at room temperature for 4-6 h. 5 μm cryosections of the matrix were cut perpendicular to the matrix layer as described above, briefly washed (with PBS and 2 mM $CaCl_2$, 150 mM NaCl, pH~7.5), sealed between two 2 mm BaF_2 windows in a flow-through high definition infra-red (HDIR) chamber [36] thermostated at 20.0°C, and hydrated in a $CaCl_2$-NaCl-NaF (CNF) solution (2 mM $CaCl_2$, 150 mM NaCl, 10 μm NaF, pH~7.5).

Microscopy and Raman micro-spectroscopy

Fluorescence and transmission (bright-field and polarized) images of longitudinal bone sections (middle 1/3 of the anterior and posterior segments marked by dashed lines in Fig. 3B) mounted in quartz slide/coverslip sandwiches and hydrated with PBS (to reduce light scattering artifacts) were recorded in a Senterra Raman microscope (Bruker Optics) with 10x/0.3NA and 40x/0.95NA objectives. For polarized images, the polarizer was oriented at 0 or 45 degrees to the periosteal surface of each section and the analyzer was oriented at 90 degrees to the polarizer. Mineral apposition rate (MAR) was measured as the distance between centers of the fluorescent lines produced by the first and second calcein injections divided by the time interval between these injections. Raman spectra from 200 to 4500 cm^{-1} were collected with 9-16 cm^{-1} resolution within posterior sections that had three distinguishable calcein labeling lines on the periosteal side, using a 40x/0.95NA objective and 532 nm circularly-polarized laser set to produce 11 mW power at the sample. The measurement points were selected every 1-2 μm along ~30 μm stripes, as illustrated by red dots in Fig. 4A. 3-7 stripes per sample were analyzed, to evenly represent the entire range of MAR observed within regions with three distinguishable labels. The spectra were corrected for the spectral throughput of the spectrometer as well as for water and quartz contributions (Supplementary Fig. S6). The mineral:organics ratio was determined from integral intensities of baseline-corrected spectral peaks of ν_1 stretching vibration of PO_4^{3-} group (915-984 cm^{-1}) and stretching vibrations of CH groups of all organic molecules (2830-3028 cm^{-1}), as described in Supplementary Fig. S6 [6, 37, 38]. To confirm the lack of polarization artifacts, the same ratio was evaluated by least-square decomposition of the spectra in the 350-1750 cm^{-1} region on mineralized and demineralized bone matrix recorded at various orientations and laser and analyzer polarizations. The collagen:organics ratio was determined from the amide III peak (1212-1306 cm^{-1}) dominated by collagen and from the CH-stretching peak.

Hyper-spectral HDIR imaging

Matrix sections mounted in the HDIR chamber were flushed with toluidine blue solution in CNF, to stain cells and matrix. Visible transmission images were recorded via a reflective 15x/0.4NA objective in a Hyperion 3000/Vertex 70 infrared microscope/spectrometer (Bruker Optics). Sections were de-stained by flushing CNF solution, and hyper-spectral infrared images were recorded for 30 min with 4cm^{-1} spectral and 2.8 μm pixel resolutions via the infrared microscope equipped with a 128×128 array detector as described in [36]. The infrared absorption spectra at each pixel were corrected for water contribution. Apparent

collagen density at each pixel was evaluated from the characteristic 1340cm^{-1} peak (baseline-corrected and integrated between 1327-1360 cm^{-1}), which is insensitive to IR light polarization and is negligible in cells (Supplementary Fig. S7) [36]. Average collagen density in the matrix was calculated by integrating the apparent densities at pixels along 14 μm wide strips perpendicular to the section where 2-3 cells were present, accounting for the section thickness and correcting for the volume occupied by cells measured from the visible images of the stained sections. Hydration of the sections with CNF solution reduced sample preparation and spectral artifacts associated with section shrinkage and broadening of the infrared peaks and light scattering [36].

Electron microscopy

Freshly dissected lumbar vertebrae (L2) from LP and RP diet animals were pre-fixed in freshly prepared 0.7% formaldehyde, 0.7 × PBS for 24 h at room temperature followed by 24 h in 2.5% glutaraldhyde, 0.12 M Na-cacodylate, pH7.3 at room temperature. Fixed vertebrae were demineralized in 50 mM EDTA, 0.12 M Na-cacodylate, postfixed in 2% OsO4, processed into Spurr's epoxy, sectioned, stained with UO2-acetate and Pb-citrate, and examined in a JEOL 1400 electron microscope at NICHD Imaging core.

Statistical analysis

Sample size of 5 animals per group was selected to ensure sufficient statistical power for effects larger than 2 SD (powering the study for 1 SD effects would require 17 animals per group). We used two-way ANOVA (hereafter ANOVA) for statistical analysis of two-factor (genotype and diet) experiments after Shapiro-Wilk normality test and Brown-Forsythe equal variance test. For *post hoc* pairwise comparisons of genotype effects within the same diet and diet effects within the same genotype, we utilized the Holm-Sidak method. We also performed the latter comparisons with a two-tail heteroscedastic Student's t-test (hereafter t-test). The latter test utilizes fewer assumptions and often yields larger p-values. Supplementary Tables S1-S5 provide full results of both analyses.

We considered a difference between two mean values to be statistically significant when the larger (more conservative) of the p-values calculated from ANOVA and t-test was smaller than 0.05. The value of the corresponding test power between 0.8 and 1.0 confirms sufficient number of measurements for reaching this conclusion. We report the number of measurements for each data set and plot error bars based on SE, thereby providing confidence intervals for visual evaluation of differences between the mean values.

Supplementary Material

Refer to Web version on PubMed Central for supplementary material.

Acknowledgments

This work was funded in part by the Intramural Research Program of the National Institute of Child Health and Human Development (NICHD), National Institutes of Health. Electron Microscopy was performed at the Microscopy and Imaging Core of NICHD with the assistance of Lynne Holtzclaw and Louis (Chip) Dye.

References

1. Shapiro, JR.; Byers, PH.; Glorieux, FH.; Sponseller, PD., editors. Osteogenesis Imperfecta. Elsevier; Amsterdam: 2014. p. 555
2. Tosi LL, Warman ML. Mechanistic and therapeutic insights gained from studying rare skeletal diseases. Bone. 2015; 76:67–75. [PubMed: 25819040]
3. Marini JC, Reich A, Smith SM. Osteogenesis imperfecta due to mutations in non-collagenous genes: lessons in the biology of bone formation. Curr Opin Pediatr. 2014; 26:500–507. [PubMed: 25007323]
4. Glorieux FH, Moffatt P. Osteogenesis imperfecta, an ever-expanding conundrum. J Bone Miner Res. 2013; 28:1519–1522. [PubMed: 23696068]
5. Marini JC, et al. Consortium for osteogenesis imperfecta mutations in the helical domain of type I collagen: regions rich in lethal mutations align with collagen binding sites for integrins and proteoglycans. Hum Mutat. 2007; 28:209–221. [PubMed: 17078022]
6. Daley E, Streeten EA, Sorkin JD, Kuznetsova N, Shapses SA, Carleton SM, Shuldiner AR, Marini JC, Phillips CL, Goldstein SA, Leikin S, McBride DJ Jr. Variable bone fragility associated with an Amish COL1A2 variant and a knock-in mouse model. J Bone Miner Res. 2010; 25:247–261. [PubMed: 19594296]
7. Mirigian LS, Makareeva E, Mertz EL, Omari S, Roberts-Pilgrim AM, Oestreich AK, Phillips CL, Leikin S. Osteoblast malfunction caused by cell stress response to procollagen misfolding in a2(I)-G610C mouse model of osteogenesis imperfecta. J Bone Miner Res. 2016; doi: 10.1002/jbmr.2824
8. Jacobsen CM, Barber LA, Ayturk UM, Roberts HJ, Deal LE, Schwartz MA, Weis M, Eyre D, Zurakowski D, Robling AG, Warman ML. Targeting the LRP5 pathway improves bone properties in a mouse model of osteogenesis imperfecta. J Bone Miner Res. 2014; 29:2297–2306. [PubMed: 24677211]
9. Grafe I, et al. Excessive transforming growth factor-beta signaling is a common mechanism in osteogenesis imperfecta. Nat Med. 2014; 20:670–675. [PubMed: 24793237]
10. Jeong Y, Carleton SM, Gentry BA, Yao X, Ferreira JA, Salamango DJ, Weis M, Oestreich AK, Williams AM, McCray MG, Eyre DR, Brown M, Wang Y, Phillips CL. Hindlimb Skeletal Muscle Function and Skeletal Quality and Strength in +/G610C Mice With and Without Weight-Bearing Exercise. J Bone Miner Res. 2015; 30:1874–1886. [PubMed: 25829218]
11. Makareeva, E.; Leikin, S. Collagen Structure, Folding and Function. In: Shapiro, JR.; Byers, PH.; Glorieux, FH.; Sponseller, PD., editors. Osteogenesis Imperfecta. Elsevier; Amsterdam: 2014. p. 71-84.
12. Grumati P, Coletto L, Sabatelli P, Cescon M, Angelin A, Bertaggia E, Blaauw B, Urciuolo A, Tiepolo T, Merlini L, Maraldi NM, Bernardi P, Sandri M, Bonaldo P. Autophagy is defective in collagen VI muscular dystrophies, and its reactivation rescues myofiber degeneration. Nat Med. 2010; 16:1313–1320. [PubMed: 21037586]
13. Gioia R, et al. Impaired osteoblastogenesis in a murine model of dominant osteogenesis imperfecta: a new target for osteogenesis imperfecta pharmacological therapy. Stem Cells. 2012; 30:1465–1476. [PubMed: 22511244]
14. Ishida Y, Yamamoto A, Kitamura A, Lamande SR, Yoshimori T, Bateman JF, Kubota H, Nagata K. Autophagic elimination of misfolded procollagen aggregates in the endoplasmic reticulum as a means of cell protection. Mol Biol Cell. 2009; 20:2744–2754. [PubMed: 19357194]
15. Martin, RB.; Burr, DB.; Sharkey, NA. Skeletal tissue mechanics. Springer; New York: 1998. p. 395
16. Pritchard, JJ. General anatomy and histology of bone. In: Bourne, GH., editor. The biochemistry and physiology of bone. Academic Press; New York: 1956. p. 1-26.
17. Currey JD. The many adaptations of bone. J Biomech. 2003; 36:1487–1495. [PubMed: 14499297]
18. Wagermaier W, Klaushofer K, Fratzl P. Fragility of Bone Material Controlled by Internal Interfaces. Calcif Tissue Int. 2015; 97:201–212. [PubMed: 25772807]
19. Carriero A, Zimmermann EA, Paluszny A, Tang SY, Bale H, Busse B, Alliston T, Kazakia G, Ritchie RO, Shefelbine SJ. How tough is brittle bone? Investigating osteogenesis imperfecta in mouse bone. J Bone Miner Res. 2014; 29:1392–1401. [PubMed: 24420672]

20. Sinder BP, Salemi JD, Ominsky MS, Caird MS, Marini JC, Kozloff KM. Rapidly growing Brtl/+ mouse model of osteogenesis imperfecta improves bone mass and strength with sclerostin antibody treatment. Bone. 2015; 71:115–123. [PubMed: 25445450]
21. Boyde A, Travers R, Glorieux FH, Jones SJ. The mineralization density of iliac crest bone from children with osteogenesis imperfecta. Calcif Tissue Int. 1999; 64:185–190. [PubMed: 10024373]
22. Forlino A, Porter FD, Lee EJ, Westphal H, Marini JC. Use of the Cre/lox recombination system to develop a non-lethal knock-in murine model for osteogenesis imperfecta with an alpha1(I) G349C substitution. Variability in phenotype in BrtlIV mice. J Biol Chem. 1999; 274:37923–37931. [PubMed: 10608859]
23. Fratzl-Zelman N, Misof BM, Klaushofer K, Roschger P. Bone mass and mineralization in osteogenesis imperfecta. Wien Med Wochenschr. 2015; 165:271–277. [PubMed: 26208477]
24. Kozloff KM, Carden A, Bergwitz C, Forlino A, Uveges TE, Morris MD, Marini JC, Goldstein SA. Brittle IV mouse model for osteogenesis imperfecta IV demonstrates postpubertal adaptations to improve whole bone strength. J Bone Miner Res. 2004; 19:614–622. [PubMed: 15005849]
25. Reilly DT, Burstein AH. The elastic and ultimate properties of compact bone tissue. J Biomech. 1975; 8:393–405. [PubMed: 1206042]
26. Burstein AH, Zika JM, Heiple KG, Klein L. Contribution of collagen and mineral to the elastic-plastic properties of bone. J Bone Joint Surg Am. 1975; 57:956–961. [PubMed: 1184645]
27. Fedarko NS, Moerike M, Brenner R, Robey PG, Vetter U. Extracellular matrix formation by osteoblasts from patients with osteogenesis imperfecta. J Bone Miner Res. 1992; 7:921–930. [PubMed: 1442206]
28. Coleman RM, Aguilera L, Quinones L, Lukashova L, Poirier C, Boskey A. Comparison of bone tissue properties in mouse models with collagenous and non-collagenous genetic mutations using FTIRI. Bone. 2012; 51:920–928. [PubMed: 22910579]
29. Rauch F, Travers R, Parfitt AM, Glorieux FH. Static and dynamic bone histomorphometry in children with osteogenesis imperfecta. Bone. 2000; 26:581–589. [PubMed: 10831929]
30. Frost HM. On the pathogenesis of osteogenesis imperfecta: some insights of the Utah paradigm of skeletal physiology. J Musculoskelet Neuronal Interact. 2003; 3:1–7. [PubMed: 15758360]
31. Forlino A, Kuznetsova NV, Marini JC, Leikin S. Selective retention and degradation of molecules with a single mutant alpha1(I) chain in the Brtl IV mouse model of OI. Matrix Biol. 2007; 26:604–614. [PubMed: 17662583]
32. Forlino A, Tani C, Rossi A, Lupi A, Campari E, Gualeni B, Bianchi L, Armini A, Cetta G, Bini L, Marini JC. Differential expression of both extracellular and intracellular proteins is involved in the lethal or nonlethal phenotypic variation of BrtlIV, a murine model for osteogenesis imperfecta. Proteomics. 2007; 7:1877–1891. [PubMed: 17520686]
33. Dandekar A, Mendez R, Zhang K. Cross talk between ER stress, oxidative stress, and inflammation in health and disease. Methods Mol Biol. 2015; 1292:205–214. [PubMed: 25804758]
34. Suire C, Brouard N, Hirschi K, Simmons PJ. Isolation of the stromal-vascular fraction of mouse bone marrow markedly enhances the yield of clonogenic stromal progenitors. Blood. 2012; 119:e86–95. [PubMed: 22262767]
35. Aaron JE, Carter DH. Rapid preparation of fresh-frozen undecalcified bone for histological and histochemical analysis. J Histochem Cytochem. 1987; 35:361–369. [PubMed: 2434557]
36. Mertz EL, Facchini M, Pham AT, Gualeni B, De Leonardis F, Rossi A, Forlino A. Matrix disruptions, growth, and degradation of cartilage with impaired sulfation. J Biol Chem. 2012; 287:22030–22042. [PubMed: 22556422]
37. Panaroni C, et al. In utero transplantation of adult bone marrow decreases perinatal lethality and rescues the bone phenotype in the knockin murine model for classical, dominant osteogenesis imperfecta. Blood. 2009; 114:459–468. [PubMed: 19414862]
38. Balooch G, Balooch M, Nalla RK, Schilling S, Filvaroff EH, Marshall GW, Marshall SJ, Ritchie RO, Derynck R, Alliston T. TGF-beta regulates the mechanical properties and composition of bone matrix. Proc Natl Acad Sci U S A. 2005; 102:18813–18818. [PubMed: 16354837]

Highlights

- Deficient osteoblast function alters bone modeling in a G610C mouse model of OI.
- It leads to reduced collagen density and hypermineralization of lamellar bone.
- It disrupts cortical drift, trapping poorly structured woven bone.
- Altered composition and structure reduce bone plasticity and make it brittle.
- Osteoblast function in G610 mice might be improved by enhancing autophagy.

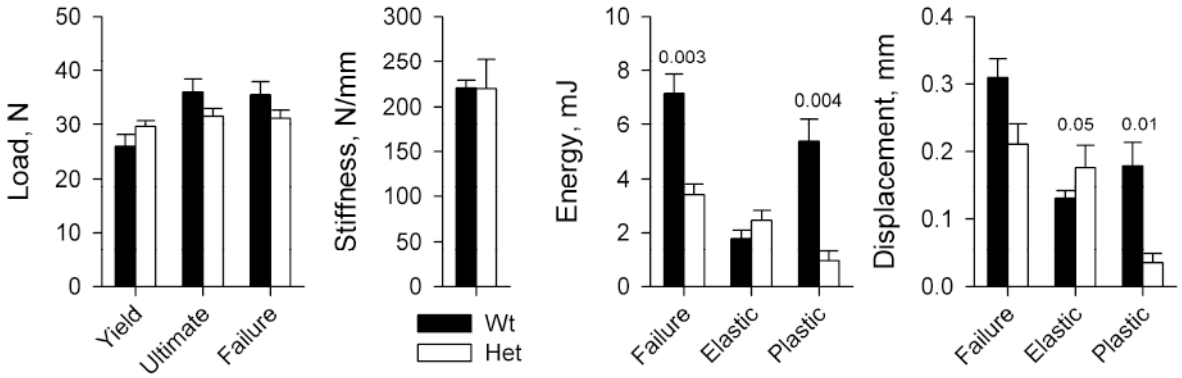

Figure 1.

Key mechanical parameters of right femurs from Wt (N=5) and Het (N=5) RP diet animals in 4-point bending tests. Yield, Failure, and Ultimate loads represent the applied force at the beginning of non-elastic (non-linear) displacement, at bone failure, and at maximum applied force prior to failure, respectively. Stiffness is the slope of the load vs. displacement curve within the elastic (linear) region. Energies are the areas under the load vs displacement curve within the linear (Elastic) and post-yield (Plastic) regions as well as overall (Failure), which represent the work of overcoming elastic, plastic and total resistance of bone to the applied forces. Hereafter, the error bars show the standard error of the mean value (SE) and the numbers above the error bars show statistically significant ($p<0.05$) and borderline ($p<0.1$) p-values. The p-values show the more conservative of two estimates: (i) two-way ANOVA (presumes equal variances) and (ii) two-tail heteroscedastic Student's t-test (presumes unequal variances). Full results of the statistical analysis are presented in Supplementary Table S1.

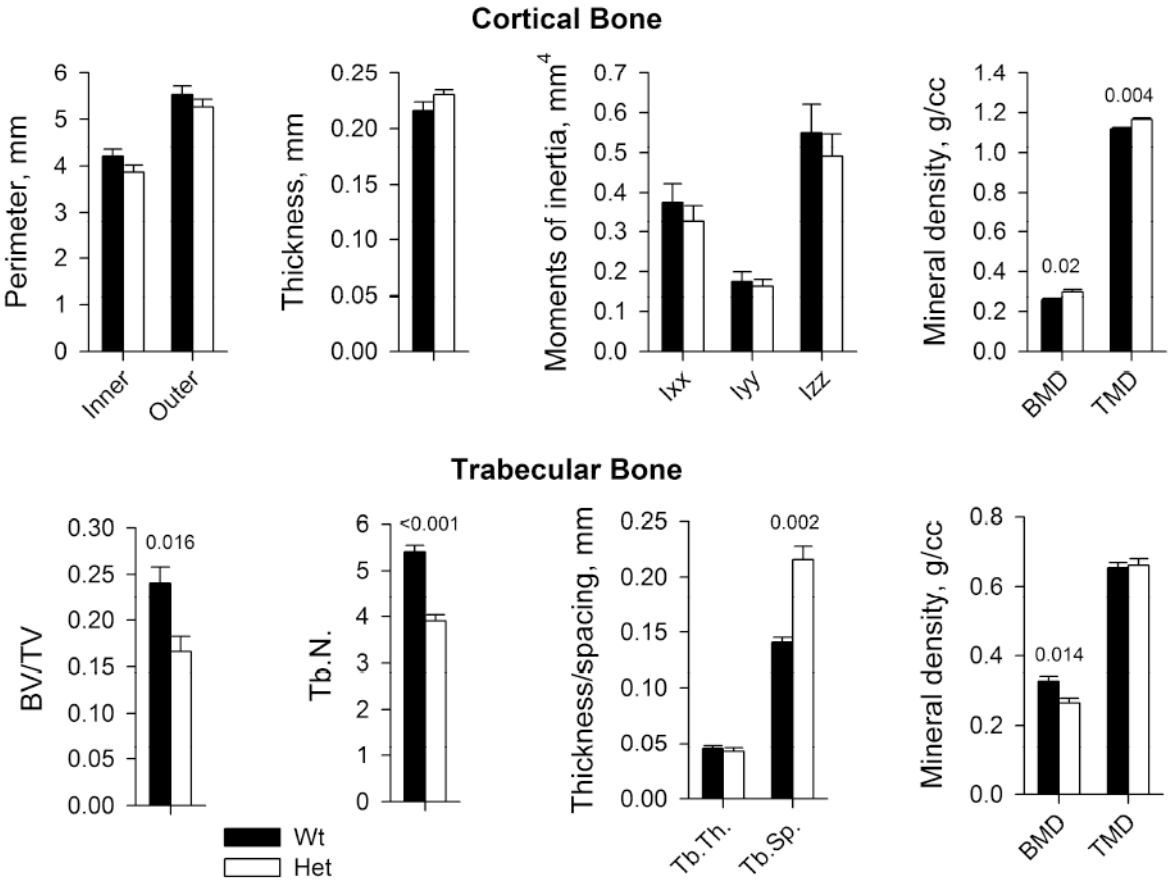

Figure 2.

Geometry and mineral density of cortical and trabecular bone in Wt (N=5) and Het (N=5) femurs used for the 4-point bending tests in Fig. 1. BMD and TMD represent the amount of mineral per total femur volume and cortical bone volume at mid-diaphysis, respectively. BV/TV is the fraction of tissue volume occupied by bone. Tb.N, Tb.Th and Tb.S are the number, thickness and spacing between trabeculae within the latter region, respectively. The error bars and p-values are defined as in Fig. 1. Full results of the statistical analysis are presented in Supplementary Table S2.

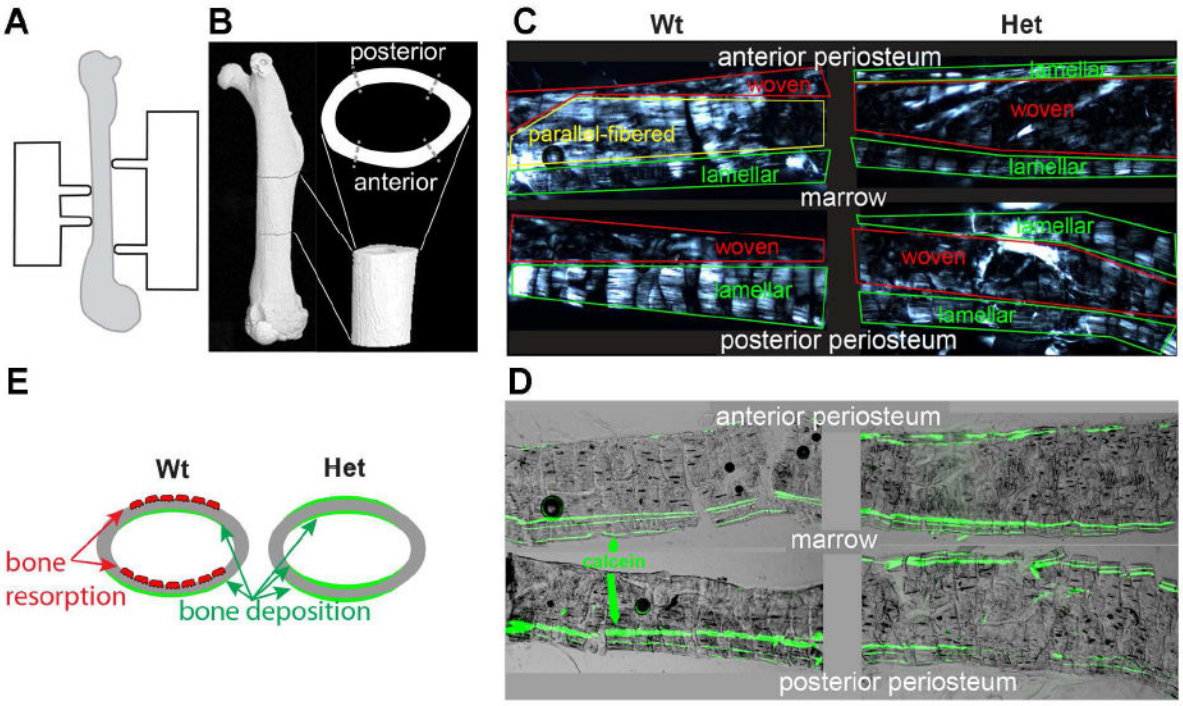

Figure 3.

Cortical bone modeling and structure at femur mid-diaphysis. **A.** Schematic illustration of a 4-point bending test setup. **B.** μCT reconstruction of femur, showing the region of mechanical testing in lateral and axial projections (both rotated 90 deg about the long axis, relative to panel A). **C.** Longitudinal sections of anterior and posterior mid-diaphysis imaged between crossed polarizers, showing regions of lamellar, parallel-fibered and woven bone. In lamellar bone, birefringent collagen fibers are mostly straight and parallel to the bone surface yet regularly rotate about the normal to the surface in a plywood-like pattern, resulting in periodic bright and dark stripes in the polarized image. In parallel-fibered bone, the fibers are almost as straight and well organized but they do not exhibit regular rotation and remain mostly parallel to the bone axis. In woven bone, which is not well organized, bundles of fibers are oriented in all directions. These three distinct bone types often transition into each other gradually, resulting in intermediate structures. **D.** Overlaid fluorescence and bright-field images of the same bone sections with clearly visible green lines of calcein fluorescence. Three parallel calcein lines are observed within region of consistent bone deposition during the diet. Two, one or no calcein lines near bone surface indicate inconsistent bone deposition, a mix of deposition and resorption or prevalent resorption. **E.** Schematic illustration of anterior to posterior drift in Wt and Het animals. Red osteoclasts depict regions of prevalent bone resorption; green color depicts regions of prevalent new bone deposition.

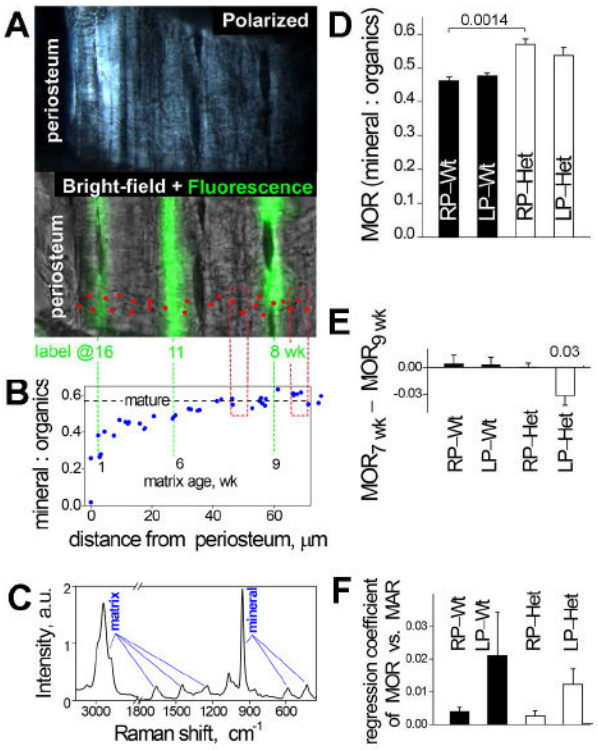

Figure 4.

Mineral content of cortical bone. **A.** Polarized and bright-field/fluorescence images of a bone section in a Raman microscope. Red dots mark the spots of Raman spectra measurements. **B.** Mineral:organics ratio (MOR) measured from Raman spectra at these spots. The dashed horizontal line shows MOR in mature matrix. Extensions of the calcein lines show the matrix age, which is calculated as the difference between the animal age at the time of sacrifice and the time of calcein injection. Red boxes mark the regions approximately 1 wk before and 1 wk after the first injection. **C.** Representative Raman spectrum measured at one of the spots. MOR values were determined from integral intensities of characteristic spectral peaks of organic matrix and mineral as described in Methods. **D.** Average MOR in maturely mineralized matrix deposited at ~ 1 wk after the diet start in Wt RP (N=4), Het RP (N=5), Wt LP (N=5), and Het LP (N=5) animals. **E.** Diet effect on the MOR in maturely mineralized matrix. To reduce effects associated with MOR variations between different bone formation sites (Supplementary Fig. S3), the diet effect was calculated as the difference in the MOR 1 wk after (MOR_{9wk}) and 1 wk before (MOR_{7wk}) the start of the diet at the same site. The resulting values were then averaged over different sites and animals within each group. With this analysis, we observed a statistically significant LP diet effect on Het animals and no diet effects in other groups. A consistent trend was observed in MOR 1wk after the diet start even when the absolute MOR values were more crudely averaged over different animals (panel D), but it did not reach statistical significance. **F.** MOR dependence on the apparent mineral apposition rate (MAR, measured from the distance between the first and second calcein injection lines). Significant axial and meridional variation in apparent MAR at femur mid-diaphysis of our mice sites precluded accurate measurement of average MAR but enabled us to test whether MOR depends on

MAR by comparing sites with different MAR within the same animal (Supplementary Fig. S3). The corresponding regression coefficient was not statistically different from zero. Full results of the statistical analysis are presented in Supplementary Table S3.

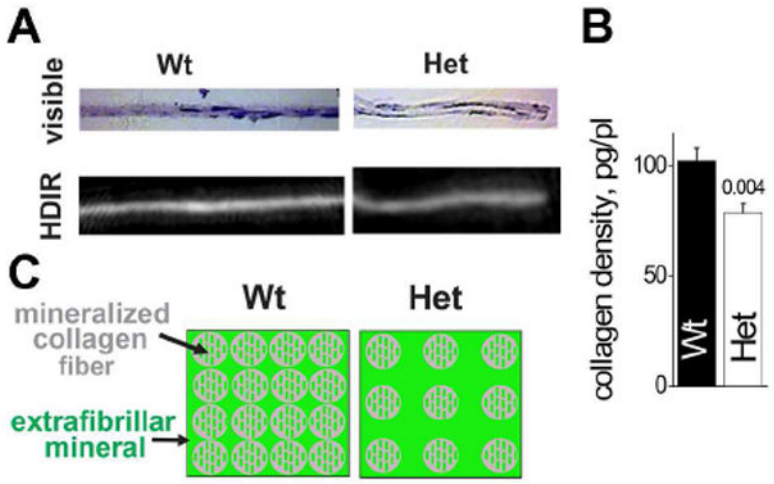

Figure 5.

Density of collagen in extracellular matrix. **A.** Visible and HDIR images of transversal sections of matrix grown in Wt and Het osteoblast cultures. Brightness of each pixel in the HDIR image is proportional to collagen amount calculated from the HDIR pixel spectrum. **B.** Average collagen density in Wt and Het samples measured by HDIR within the matrix space between cells. **C.** Matrix hypermineralization model, in which excessive mineral is deposited in the interstitial space between collagen fibers.

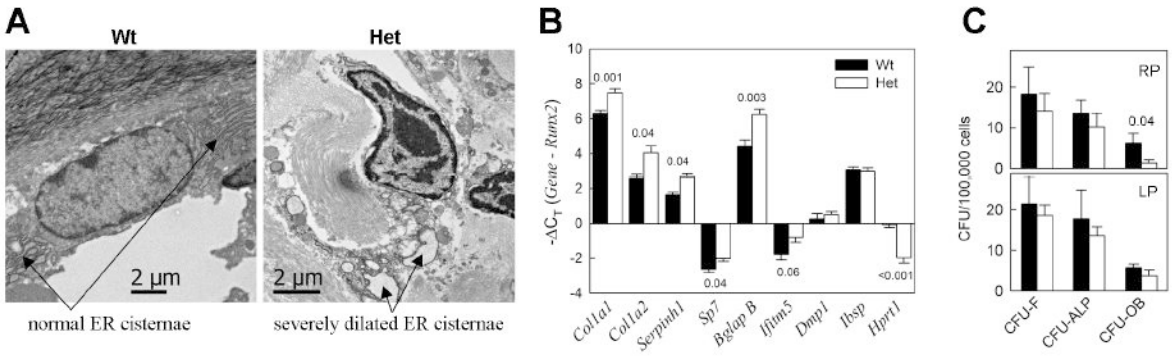

Figure 6.

Osteoblast cell stress. **A.** Electron microscopy images of lumbar vertebrae osteoblasts in RP diet animals, illustrating severe ER dilation in Het osteoblasts. **B.** qPCR analysis of gene transcription in frontal bone of Wt and Het calvaria (see Supplementary Table S4 for full statistical analysis). Since no systematic differences between gene transcription in RP and LP animals were observed (Supplementary Fig. S5), the animals from both diet groups were pooled together (in each genotype, N=4 for *Col1a2* and *Serpinh1*and N=10 for all other genes). **C.** Differentiation of BMSCs from RP and LP animals in culture at identical conditions (3 animals in each group and 6 wells/animal in each CFU experiment were examined, see Supplementary Table S5 for statistical analysis).

Table 1

Mineral and matrix contents in bone and in extracellular matrix of calvarial osteoblast cultures measured or estimated by different methods.

Het : Wt ratios					
Mineral content (bone)		**Matrix content (bone)**			**Collagen density (matrix in culture) HDIR**
TMD µCT	**mineral:organics µRaman**	**collagen:organics µRaman**	**organics density***		
			µCT&µRaman	**µRaman**	
1.04 ± 0.02#	1.161–24#	0.93-0.99	0.84–0.90#	0.86–0.94#	0.77 ± 0.06#

*Estimated from our µCT and/or Raman data as described in Supplementary Data Analysis.

#The difference between Het and Wt is statistically significant (the ratios are larger or smaller than 1 with $p<0.05$).